Observations of the Development and Vertical Structure of the Lake-Breeze Circulation during the 2017 Lake Michigan Ozone Study

TIMOTHY J. WAGNER,[a] ALAN C. CZARNETZKI,[b] MEGAN CHRISTIANSEN,[c] R. BRADLEY PIERCE,[a,d] CHARLES O. STANIER,[c] ANGELA F. DICKENS,[e] AND EDWIN W. ELORANTA[a]

[a] *Cooperative Institute for Meteorological Satellite Studies, Space Science and Engineering Center, University of Wisconsin–Madison, Madison, Wisconsin*
[b] *Department of Earth and Environmental Sciences, University of Northern Iowa, Cedar Falls, Iowa*
[c] *Department of Chemical and Biochemical Engineering, University of Iowa, Iowa City, Iowa*
[d] *Department of Atmospheric and Oceanic Science, University of Wisconsin–Madison, Madison, Wisconsin*
[e] *Lake Michigan Air Directors Consortium, Hillside, Illinois*

(Manuscript received 2 October 2020, in final form 20 December 2021)

ABSTRACT: Ground-based thermodynamic and kinematic profilers were placed adjacent to the western shore of Lake Michigan at two sites as part of the 2017 Lake Michigan Ozone Study. The southern site near Zion, Illinois, hosted a microwave radiometer (MWR) and a sodar wind profiler, while the northern site in Sheboygan, Wisconsin, featured an Atmospheric Emitted Radiance Interferometer (AERI), a Doppler lidar, and a High Spectral Resolution Lidar (HSRL). Each site experienced several lake-breeze events during the experiment. Composite time series and time–height cross sections were constructed relative to the lake-breeze arrival time so that commonalities across events could be explored. The composited surface observations indicate that the wind direction of the lake breeze was consistently southeasterly at both sites regardless of its direction before the arrival of the lake-breeze front. Surface relative humidity increased with the arriving lake breeze, though this was due to cooler air temperatures as absolute moisture content stayed the same or decreased. The profiler observations show that the lake breeze penetrated deeper when the local environment was unstable and preexisting flow was weak. The cold air associated with the lake breeze remained confined to the lowest 200 m of the troposphere even if the wind shift was observed at higher altitudes. The evolution of the lake breeze corresponded well to observed changes in baroclinicity and calculated changes in circulation. Collocated observations of aerosols showed increases in number and mass concentrations after the passage of the lake-breeze front.

KEYWORDS: Inland seas/lakes; Lake effects; Sea breezes; Lidars/Lidar observations; Profilers, atmospheric; Air quality

1. Introduction

It is well known that the Laurentian Great Lakes have a significant impact on the weather and climate of the upper midwestern United States. These large bodies of water (which collectively encompass approximately 18% of the world's supply of liquid freshwater) force changes in temperature, cloud cover, and precipitation with significant diurnal and seasonal variability (Scott and Huff 1996), and the impacts of the lakes can even extend to severe convective weather (King et al. 2003). The lake-breeze circulation is one of the most important mechanisms for latent and sensible heat exchange between the lakes and the surrounding environment. This is, in part, due to common occurrence of the Great Lakes lake breezes. For example, Laird et al. (2001) constructed a 15-yr climatology of Lake Michigan lake-breeze events and found that lake breezes tended to occur more frequently as the summer progressed. Depending on the location, lake-breeze frequency increased from 5 to 9 events per month in May to 8 to 12 per month in August. Other studies have used different criteria to identify lake breezes and found higher frequencies. Lyons (1972) showed that Chicago, Illinois, experienced a lake breeze on approximately half of all days in May through September. With events occurring multiple times a week during the warm months, operational forecasters need to be familiar with their formation, structure, and impacts, while numerical weather prediction and air quality models must be able to simulate them properly.

Since a substantial fraction of the world's population lives in coastal regions, sea and lake breezes have been a subject of interest to humanity since antiquity (Simpson 1994; Miller et al. 2003) and the broad outlines of their formation have been known for generations. Due to water's large heat capacity, its ability to absorb solar energy over a finite depth, and the vertical mixing present in large bodies of water, surface temperatures respond slowly to solar heating. On the seasonal time scale, peak lake surface temperatures lag their terrestrial counterparts by several weeks while on diurnal scales lake temperatures are typically colder than land during the day but warmer at night. As a result, a sharp land–water gradient in the temperature and density of the near-surface air can arise, inducing a circulation as the atmosphere attempts to restore equilibrium. This circulation is commonly found where the body of water has sufficient thermal mass relative to the land. While the sea breeze and Great Lakes breezes are well

Corresponding author: Timothy J. Wagner, tim.wagner@ssec.wisc.edu

DOI: 10.1175/JAS-D-20-0297.1

known, lake breezes have also been observed for both natural lakes and reservoirs with length scales of just a few kilometers (Segal et al. 1997).

A robust solenoidal-based explanation of the lake-breeze circulation has emerged (Holton 1992; Miller et al. 2003; Martin 2006). The Bjerknes circulation theorem states that the material (Lagrangian) change in the absolute circulation C_a of a fluid element can be described as

$$\frac{dC_a}{dt} = -\oint \frac{dP}{\rho}, \tag{1}$$

where P is pressure and ρ is density. In the special case of a barotropic fluid, density is a function of pressure alone and the right-hand side reduces to the closed line integral of an exact differential (which is zero). Thus, Bjerknes's circulation theorem is merely a more general case of Kelvin's circulation theorem, which states that the absolute circulation in a barotropic fluid is conserved. However, the differential heating present at a lake or sea boundary ensures that the environment is far from barotropic: the daytime geopotential heights are greater over the land, and thus isobars slope downward toward the cooler water while isopycnals (lines of constant density) slope toward warmer land. This ensures that the environment is baroclinic. The horizontal flow both at the surface and aloft is isobaric and does not contribute to the circulation change, as $dp = 0$ for those branches. However, as the daytime ascending branch (over land) and the descending branch (over water) are associated with environments with very different densities, there is a net difference between these two branches and thus an acceleration along the perimeter of the fluid element is induced. This is a thermally direct circulation, and over time the vertical motions would be expected to reduce the baroclinicity of the environment as the isopycnals would be rotated to be more parallel to the isobars. At night, a weak land breeze can develop when the temperature gradient is reversed.

Changes in the thermodynamic structure of the environment accompany the changes in the kinematics described above. The development of onshore flow at low levels produces cold-air advection. The flow of this comparatively denser air from water to land takes the form of a localized gravity current (Miller et al. 2003). The cooler air inhibits convection, producing clearing skies that can be seen on satellite imagery; a characteristic example of this is depicted in Fig. 1. Since temperatures above the gravity current are not affected, a shallow inversion will develop (Keen and Lyons 1978).

The present study comprehensively describes the temporal and vertical development of the lake-breeze circulation on the western shore of Lake Michigan using data collected during the 2017 Lake Michigan Ozone Study (LMOS 2017; Stanier et al. 2021). The development and structure of western Lake Michigan breezes have been of considerable interest (e.g., Lyons 1972; Keen and Lyons 1978; Sills et al. 2011), likely due in part to the large population centers located along the lake shore. One aspect of the relationship between these major urban areas and the lake is the adverse impacts that lake breezes have on air quality, as they have

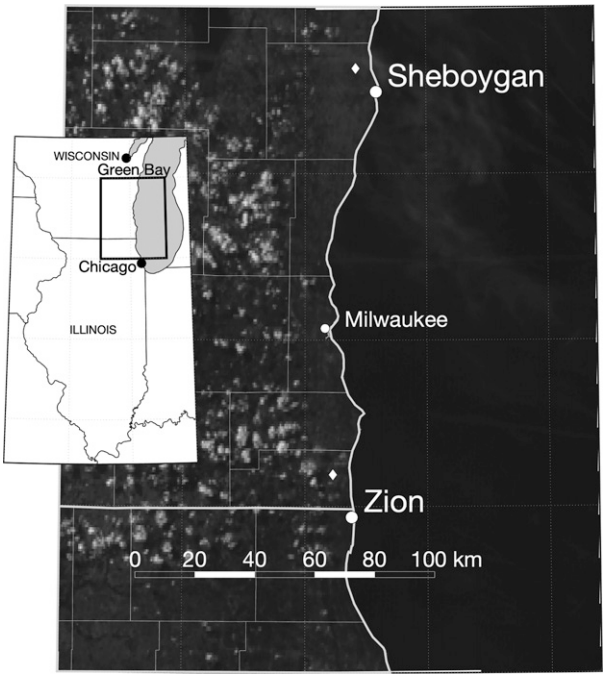

FIG. 1. Location of the Sheboygan and Zion supersites along the shore of Lake Michigan, overlaid on *GOES-16* 0.64-μm reflectance at 2112 UTC 2 Jun 2017. Small white diamonds indicate the location of inland monitoring sites used to determine lake-breeze penetration. The cities of Chicago, Milwaukee, and Green Bay are shown for reference. The satellite imagery depicts the lack of convective clouds adjacent to the lake shore frequently seen with mature lake breezes.

been shown to play a significant role in the production and transport of ground-level ozone in shoreline communities along Lake Michigan (Lyons and Cole 1976; Dye et al. 1995; Levy et al. 2010). Ozone precursors emitted from densely populated regions are transported over the lake. So long as the precursors remain offshore, the shoreline communities are not impacted by increased ozone production. When the lake breeze is present, however, ozone and its precursors are transported inland and convergence along the lake-breeze boundary results in significant increases to observed ozone concentrations. The deployment of high-temporal-resolution thermodynamic and kinematic profilers alongside aerosol lidars, air samplers, and other instruments, at two sites adjacent to Lake Michigan in support of LMOS 2017, allows the investigation of lake-breeze events from a novel perspective. While other studies have investigated the kinematic characteristics of lake and sea breezes using higher-temporal-resolution profiling instruments like Doppler lidars (e.g., Curry et al. 2017; Banta et al. 1993) and sodars (e.g., Mastrantonio et al. 1994; Prakash et al. 1992), the present work introduces continuous thermodynamic profiling using instruments observing both microwave and infrared emission. When coupled with collocated wind profiling instruments, a detailed picture of the thermodynamic and aerosol characteristics of the lake-breeze circulation and its

evolution emerges. Wind and thermodynamic profiles from lake-breeze events are composited on an event-centric time scale to capture the behavior of the atmosphere before and after lake-breeze arrival; a similar technique has been used to investigate the near-storm environment of severe storms (Wagner et al. 2008) and bores (Loveless et al. 2019). The remainder of this paper describes the field campaign and the instruments (section 2), explores the evolution of surface weather conditions (section 3), vertical structure (section 4), and particulate air quality (section 5), and synthesizes these observations to improve understanding of lake-breeze circulations from the combined thermodynamic and kinematic perspective (section 6).

2. Measurements and instrumentation

a. The 2017 Lake Michigan Ozone Study

The LMOS 2017 was devoted to observing chemical and meteorological features important to persistently high ozone concentrations along the western shore of Lake Michigan. Project collaborators included NASA, NOAA, EPA, the Lake Michigan Air Directors Consortium (LADCO), state environmental agencies, universities, and the private sector. A significant goal of LMOS 2017 was to better understand how the unique geography and meteorology of the Lake Michigan basin drives significant ground-level ozone production even in communities with relatively low emission rates of ozone precursors. By uniting land-based, ship-based, and airborne measuring systems, a comprehensive portrait of the thermodynamic, kinematic, and chemical state of the coastal environment during high ozone events was obtained. An additional goal of the experiment was to use the data to evaluate the performance of meteorological and air quality models and inform their improvement.

The field phase of LMOS 2017 was conducted from 22 May to 22 June 2017. This period historically encompasses a significant number of ozone exceedance events for shoreline communities due to the combination of numerous lake-breeze events (as the lake has not yet warmed significantly) coupled with sufficient insolation to induce the photochemistry required for ground-level ozone production; the cold water also inhibits mixing and ensures that precursors remain near the surface. Two ground-based supersites were established. The more southerly supersite was near Zion, Illinois (roughly halfway between Chicago and Milwaukee, Wisconsin). The northern supersite was at Sheboygan, Wisconsin (about 80 km north of Milwaukee); a map depicting their locations is seen in Fig. 1. The Sheboygan site (43.745°N, 87.709°W) was within 230 m of the shore while the Zion site (42.468°N, 87.810°W, AQS 17-097-1007) was approximately 1 km inland. The lake shore has a similar north–south orientation in the vicinity of the two sites, although the shoreline is more sinuous at Sheboygan. In-depth descriptions of the two sites are found in Doak et al. (2021). Airborne platforms included the NASA UC-12, which carried remote sensing instruments for aerosols, clouds, and trace gases, and a light aircraft operated by Scientific Aviation, which conducted in situ profiling of trace gases and meteorological characteristics. The NOAA research vessel R5503 provided nearshore transects of surface meteorology and trace gas concentrations with a Pandora differential absorption optical spectrometer (Herman et al. 2009), while onshore vehicles conducted mobile sampling of terrestrial ozone and meteorology. Preliminary campaign results have been reported (Abdioskouei et al. 2019; Vermeuel et al. 2019) and analysis of this significant volume of data is ongoing.

b. Instrumentation

For the purposes of the present work, the most significant data were collected at the two supersites near Sheboygan and Zion. The Space Science and Engineering Center (SSEC) Portable Atmospheric Research Center (SPARC; Wagner et al. 2019) was deployed at Sheboygan, while a Radiometrics MP3000 and an Atmospheric Systems Corporation acoustic wind profiler, or sodar, were deployed at Zion. Surface observations at the two sites came from instruments mounted on 10-m towers, and each site also featured air quality instrumentation to measure ozone and particulate matter.

SPARC, a portable ground-based atmospheric profiling laboratory, includes an Atmospheric Emitted Radiance Interferometer (AERI; Knuteson et al. 2004a,b), a Halo Photonics Streamline XR Doppler lidar (DLID; Pearson et al. 2009), and a High Spectral Resolution Lidar (HSRL; Shipley et al. 1983; Eloranta 2005). At Sheboygan, the thermodynamic state was captured by AERI, a commercially available hyperspectral infrared radiometer that passively measures downwelling near- and thermal infrared spectra with a spectral resolution better than 1 cm^{-1} and a temporal resolution of approximately 30 s. Profiles of temperature and water vapor can be retrieved from AERI-observed spectra through the Tropospheric Remotely Observed Profiling via Optimal Estimation (TROPoe) retrieval, formerly known as AERIoe (Turner and Löhnert 2014; Turner and Blumberg 2019). TROPoe profiles have been shown to agree well with radiosondes when they originate from either an AERI (Turner and Löhnert 2014; Turner and Blumberg 2019) or a microwave radiometer (MWR; Turner and Löhnert 2021). The a priori atmospheric state for the retrieval during this deployment was calculated from a multiyear climatology of late spring and early summer radiosondes launched from the National Weather Service office at Green Bay, Wisconsin. A principal component analysis noise filter is applied to the AERI radiances to reduce noise before the retrieval is executed, in which the observations are decomposed into principal components and the spectrum is rebuilt from those that have the greatest variance (Turner et al. 2006). The DLID uses a 1.5-μm pulsed laser to capture the radial velocity of boundary layer aerosols; by scanning at a fixed zenith angle at different azimuths, it is possible to geometrically calculate the wind profile above the lidar. The HSRL is a vertically pointing lidar that uses spectral width differences to discriminate between molecular and aerosol scattering: the spectrum for aerosol backscattering is confined to the relatively narrow range of Doppler-shifted frequencies associated with vertical motions in the atmosphere

TABLE 1. Summary of the instrumentation deployed at the two ground sites used in this study. All data used in this study are publicly available at https://www-air.larc.nasa.gov/missions/lmos/.

Instrument	Deployment site	Observation type	Approximate vertical range	Temporal resolution	Uncertainty
AERI	Sheboygan	Profiles of temperature, water vapor	0–3000 m	2 min	0.9 K, 1.0 g kg^{1}
Doppler lidar	Sheboygan	Wind vector profiles	140–1200 m	1.75 min	0.4 m s^{-1}
HSRL	Sheboygan	Aerosol backscatter profiles	55–14 600 m	0.5 min	5% of observed value
Microwave radiometer	Zion	Profiles of temperature, water vapor	0–3000 m	3 min	1.6 K, 1.4 g kg^{-1}
Sodar	Zion	Wind vector profiles	30–200 m	2 min	0.5 m s^{-1}, 2°
Met One AIO	Zion	Temperature, humidity, wind	10 m	1 min	0.2 K, 3% RH, 0.5, m s^{-1}
SMPS-APS	Zion	Aerosol size distributions	5 m	20–135 s	20% of aerosol diameter
Vaisala WXT 530	Sheboygan	Temperature, humidity, wind	10 m	1 min	0.3 K, 3% RH, 3% wind speed
AERONET	Zion	Aerosol optical depth	Total column	Variable	±0.1

while the molecular spectrum is broadened by the Maxwellian thermal motion of the molecules. This allows high-precision absolutely calibrated aerosol backscatter retrievals and independent retrievals of aerosol extinction. With these instruments, SPARC is able to provide a comprehensive profile of the evolution of the atmospheric state on a time scale that is measured on the order of minutes.

At Zion, the MWR passively observed the brightness temperature of downwelling radiance in 22 channels, with eight channels measuring the water vapor absorption band and 14 channels observing the oxygen absorption band. The TROPoe algorithm was then used to retrieve profiles of water vapor and temperature from these measurements using the same prior data as were used for the Sheboygan retrievals; by using TROPoe instead of the manufacturer-supplied neural network retrievals, a more direct comparison to the AERI observations at Sheboygan could be carried out. The collocated sodar operated at audio frequencies near 4500 Hz. In sodar remote sensing, the frequency of the echo from the high-intensity acoustic pulses is directly proportional to the radial motion of the scattering volume relative to the instrument. The radial motions determined from the Doppler shift of each pulse in a set were combined to produce three-dimensional wind profiles from 30 to 200 m above ground level (AGL).

The Zion site was also home to several air quality instruments. A Scanning Mobility Particle Sizer and Aerodynamic Particle Sizer (SMPS-APS; Shen et al. 2002) system measured aerosol size distributions at the surface, covering a combined aerodynamic diameter size range of 13 nm–8354 μm. The size distributions from the APS were converted from aerodynamic to electrical mobility diameters (SMPS) and merged to the final size distribution following the method presented in Khlystov et al. (2004). Size distributions were averaged to a common 10-min time series. An Aerosol Robotic Network (AERONET; Holben et al. 1998) measuring aerosol optical depth (AOD) was also located at the Zion site from 4 to 22 June of the campaign. AERONET level 2.0 data (cloud screened and quality assured) were used in the present work (Smirnov et al. 2000). AOD was interpolated to 550 nm in the following manner:

$$\tau_{\lambda_{550}} = \tau_{\lambda_{500}}\left(\frac{\lambda_{550}}{\lambda_{500}}\right)^{-\alpha}, \tag{2}$$

where $\tau_{\lambda_{500}}$ is AOD at 500 nm and α is the angstrom exponent (440–870 nm) as reported by AERONET. The relevant characteristics of the instruments used in this study are summarized in Table 1.

c. Lake-breeze events

The following criteria were used to objectively identify the lake-breeze events (defined as the passage of a lake-breeze front) at the two sites:

1) The zonal (u) component of the surface wind reversed from offshore to onshore.
2) Surface temperatures dropped abruptly with the wind shift.
3) Mixing height decreased with the wind shift.
4) No rain was detected within three hours of the wind shift.

The cases chosen for analysis are a consequence of the selection criteria. While a set of more permissive criteria could result in a greater number of cases, events that are not unambiguously lake breezes might also be included. The mixing height criterion was included to establish that the atmospheric environment before the lake breeze was continental in character, with the air temperature being influenced by solar heating and/or warm-air advection. A decrease in the mixing height coincident with the wind shift indicates that surface air is now originating over the lake. Laird et al. (2001) identified a set of criteria to objectively identify lake breeze,

TABLE 2. Dates and times of the identified lake-breeze events for the two observation sites during LMOS 2017 as well as lake temperatures from the GLSEA analysis. Times are in UTC; local time is UTC − 5 h and local standard time is UTC − 6 h. Temperatures are in °C. Blanks represent days during which a lake breeze was observed at only one location. Boldface times represent events with inland penetration.

Date	Time at Sheboygan	Time at Zion	Sheboygan lake temperature (°C)	Zion lake temperature (°C)
2 Jun	**1542**	**1448**	9.9	11.8
8 Jun	**1449**	**1516**	10.9	13.1
11 Jun	**1432**	1752	12.1	15.0
12 Jun	1543	1730	12.1	16.1
15 Jun	—	**1720**	—	17.4
16 Jun	**1741**	1704	14.5	17.3
17 Jun	**1420**	—	14.5	—

including a change in wind direction, maximum air temperatures greater than that of the lake surface, and synoptically quiescent conditions. While the Laird et al. (2001) criteria were not specifically used as filtering criteria in the present study, all of the lake-breeze events examined here also satisfied these criteria. Some authors claim that lake breezes are associated with an identifiable lake-breeze front (e.g., Ryznar and Touma 1981) while others state that the leading edge of the lake breeze does not always have the sharp discontinuity associated with a front (e.g., Sills et al. 2011); the criteria presented here emphasize the former perspective over the latter.

The identification criteria were applied separately to the Sheboygan and Zion observations, and the time of the lake-breeze arrival (LBA), representing the moment the lake-breeze front passed over the observing sites, was defined as the time of the greatest shift in wind direction. This resulted in a total of six lake-breeze events at each location, consistent with the climatology for late spring (Laird et al. 2001). Five study days included lake breezes at both sites while 2 days had an event at only one site and not the other. On average, LBA occurred much earlier at Sheboygan (1541 UTC, 1041 local time, 0941 local standard time) than Zion (1630 UTC, 1130 local time, 1030 local standard time). However, the small number of cases and variability in arrival times at each site means this difference is not statistically significant. For the 5 days in which lake breezes were observed at both locations, the correlation in LBA was low ($r = 0.0935$). The lack of correlation between arrival times is consistent with an understanding that lake-breeze events are driven more by local conditions than by synoptic forcing. Analysis of contemporaneous surface maps (not shown) helps illustrate this last point: in all cases presented here, any synoptic-scale disturbances were either hundreds of kilometers removed from the observing sites, were stationary, or did not propagate over the observation domain until after the period analyzed in this paper. The dates and times of the observed lake breezes are shown in Table 2.

3. Composite surface conditions

An objective method to identify the timing of lake-breeze events was used to composite the individual cases observed during the LMOS 2017 campaign. For each event, the time of LBA was subtracted from the observation times so that the resulting timeline was measured relative to LBA. The observations from each instrument and event were then interpolated to a common timeline with 5-min resolution from 3 h before LBA to 3 h after; this facilitated comparisons across instruments and events. Figure 2 illustrates the results of this composite analysis for the surface conditions at the two sites. Results from Sheboygan (Zion) are shown with solid (dashed) lines. Thin colored lines represent individual events while thick black lines represent the mean of all events for a particular site. The mean wind speed and direction were calculated by first determining the mean zonal (u) and meridional (v) components of the wind, then converting to speed and direction. Overall, surface conditions were consistent with what would be expected during a lake- or sea-breeze event, though some interesting details emerged. Figure 2a exhibits the wind directions for the various events, with the wind shift used to define LBA clearly evident. Both sites have nearly identical time series for the mean wind direction, with westerly winds undergoing a rapid shift to southeasterly at LBA followed by a much slower turning toward a more southerly direction over the ensuing hours, a result of Coriolis (inertial) acceleration. Substantial variations from one event and site to the next were seen prior to LBA, but once the lake-breeze front passed, the wind directions were much more uniform. This lower variability in wind direction may be due to consistency in the onshore perturbation horizontal pressure gradient force that develops as the air over land warms, and the reduced friction surface winds experience flowing over water. The wind speed (Fig. 2b) shows substantial variability between cases and from one time step to the next. On average, the speeds were higher at Zion than Sheboygan, and while Sheboygan had little change in the mean wind speed pre- and post-LBA, the mean winds at Zion were over 1.4 times faster after LBA than before.

While the driving factor of the lake-breeze circulation is the difference between the temperatures of the air over land and water, the lack of observations of the latter means that the lake surface temperature needs to be used as a proxy. Figure 2c shows the time series for the difference between the air and lake temperature on lake-breeze days. In situ observations of the lake temperature were sparse, with no operational buoys within tens of kilometers of Sheboygan. Therefore,

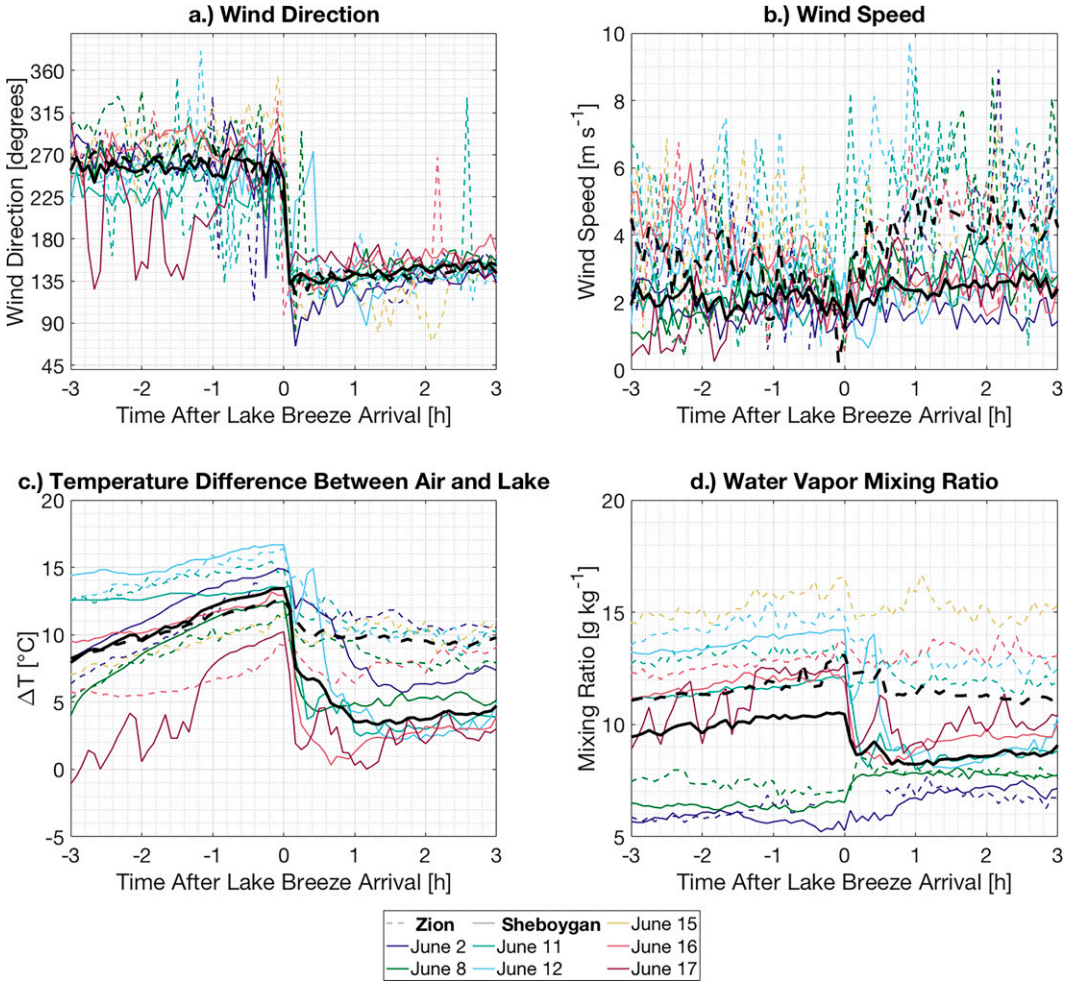

FIG. 2. Time series of composited surface conditions for the lake-breeze events analyzed in the present study, including (a) wind direction (°), (b) wind speed (m s^{-1}), (c) the difference between the air temperature and the lake surface temperature as obtained from the GLSEA analysis (°C), and (d) the water vapor mixing ratio (g kg^{-1}). Observations from Zion are depicted with a dashed line while observations from Sheboygan are shown with a solid line. The thick black lines represent the mean for each site.

lake surface temperatures were obtained from the Great Lakes Research Laboratory (GLERL) Great Lakes Surface Environmental Analysis (GLSEA; Schwab et al. 1999). Values were obtained from the GLSEA grid points located approximately 10 km from the observation sites at an azimuth of 140° (the average wind direction 1 h after LBA). The analyses were computed once per day, and these temperatures are recorded in Table 2. On average, the lake at Zion was about 3°C warmer than near Sheboygan, and during the month-long experiment seasonal warming caused a greater increase at Zion. On average the air–lake temperature difference (Fig. 2c) gradually but steadily increased at a rate that was effectively identical for both locations. Following LBA, the mean lake–land difference decreased substantially at Sheboygan, dropping from 12.2°C at LBA to 3.2°C just 1 h later. A smaller change was observed at Zion, as the mean air–lake temperature difference went from 12.1° to 9.7°C during the same period. The overall pattern for ambient air temperature was largely the same as the air–lake differences (not shown). Air temperatures at Zion tended to be warmer than at Sheboygan both before and after LBA, a function of Zion's lower latitude, a longer fetch over land to reach the observing site, and lake breezes that occurred later in the day allowing more solar heating before LBA. Absolute water vapor content (as represented by the mixing ratio, Fig. 2d) exhibited a very gradual increase in the hours before LBA consistent with typical evolution of the planetary boundary layer (PBL). The lake breeze itself had very little impact on the mixing ratio at Zion for any event, but four of the six Sheboygan events experienced a notable decrease in mixing ratio with LBA. This can be explained by the relative differences between the lake air and land air temperatures at the two sites: Zion had a much smaller difference than Sheboygan, so there was little difference between the saturation mixing

ratios following LBA. By contrast, Sheboygan experienced a significant decrease in its saturation mixing ratio following LBA due to the colder air temperatures, and so absolute water vapor content decreased even though the arriving air originated over a large body of water. By contrast, the relative humidity at both sites (not shown) showed an increase following LBA. Since the absolute humidity was constant or decreasing following LBA, this increase in relative humidity was solely driven by the decrease in air temperature.

4. Composite vertical structure

It is well known that the structure and influence of the lake-breeze circulation extends vertically beyond the near-surface level. Previous studies have used frequent balloon launches (Lyons 1972), instrumented aircraft (Finkele et al. 1995), and kinematic profilers (e.g., Curry et al. 2017; Banta et al. 1993) to investigate the vertical structure of lake-breeze circulations. However, continuous contemporaneous observations of winds, temperature, and moisture profiles during lake- and sea-breeze events have been rare. LMOS 2017 provided a unique opportunity to assess how the vertical structure of these fields evolved over time during several different lake-breeze events. The same compositing technique described earlier was applied to the vertical dimension so that structure in the PBL could be resolved. An important caveat when looking at the vertical plots of remotely sensed thermodynamic variables is that the true vertical resolution (i.e., the minimum size of an element that can be resolved by the profiler) is finer for an infrared than a microwave radiometer due to the narrower weighting functions and higher information content found in the infrared band (Ebell et al. 2013; Blumberg et al. 2015). The TROPoe retrieval can be used to quantify how well each instrument resolves both temperature and water vapor structure. On average, at the 200-m level (which is roughly the height of the post-LBA inversion), the AERI vertical resolution for temperature was approximately twice as fine as the MWR (0.25 and 0.49 km, respectively) and was approximately 2.5 times better for water vapor (1.19 and 3.00 km, respectively). Therefore, the enhanced detail in the Sheboygan time–height cross sections of thermodynamic variables is more likely due to differences in the instruments used than physical differences in the lake breeze itself.

a. Temperature and moisture structure

Time–height cross sections of temperature and mixing ratio overlaid with wind barbs are shown in Fig. 3. Observations from all instruments were interpolated onto a common grid with temporal resolution of 5 min (same as the surface composites shown earlier) and a vertical spacing of 20 m. The data from both Zion and Sheboygan illustrate that while the increase in temperature in the period leading up to LBA is greatest at the surface, increases in temperature with time were seen several hundred meters above the surface as the surface air was mixed upward. An inversion present a few hours before LBA was more easily seen in Sheboygan than Zion. There are two reasons for this: first, since the average time of LBA was earlier at Sheboygan, the 3-h period preceding LBA was more likely to include an early-morning inversion; and second, the enhanced vertical resolution of the AERI enabled the inversion at Sheboygan to be resolved with increased fidelity. Prior to LBA winds near the surface were southwesterly and veered with height, becoming northwesterly at an altitude of 1 km. Wind direction at a given height tended to be constant with time before LBA, though there was a tendency for the speeds to decrease with time. In the 30 min prior to LBA, the potential temperature gradient in the lowest 400 m (not shown) was greatly relaxed as the lower troposphere underwent significant mixing while the free troposphere remained largely adiabatic both before and after LBA. The arrival of the lake breeze resulted in a sudden decrease in temperature that was greatest at the surface but still prevalent in the lowest 100–200 m; again, this was more evident in the AERI observations at Sheboygan. A strong inversion developed post-LBA as the cold lake air advanced beneath and lifted the warmer land air. Strong marine inversions such as these are expected in the spring when the lakes are significantly colder than the nearby land. Above the inversion, the air temperature at a given height increased with time. This was likely subsidence-induced warming, caused by the descending branch of the lake-breeze circulation, which helped to enhance the strength of the inversion and increase the stability of the environment. Therefore, the cold temperatures commonly associated with the lake breeze were confined to a shallow layer in the lowest part of the troposphere even as the breeze-induced changes in wind direction extended above that height. Figure 3 also shows the mixing height calculated from the composited thermodynamic profiles. Mixing height grew throughout the morning with increased diabatic heating, and was deeper at Zion where air temperatures were warmer. However, the arrival of the lake breeze caused a sudden drop in the mixing height as the atmosphere rapidly stabilized. This has significant ramifications on air quality, as the lake-breeze circulation-induced inversion traps ozone precursors and other pollutants in the near-surface air (Dye et al. 1995; Levy et al. 2010).

These observations show a disconnect between the depth of cold air and the depth over which the lake-breeze circulation impacted wind direction. The depth of the cold air that arrived onshore was limited by the vertical extent of conductive cooling. Both observations and numerical simulations indicate that significant heat loss by conduction is limited to the lowest 150 m of the atmosphere (Lyons 1970). However, winds clearly changed above the cold pool. Before LBA, westerly surface winds indicated the synoptic-scale horizontal pressure gradient force was directed toward the northeast. With sunrise, the near-surface air over land warmed more rapidly with solar heating, producing a perturbation horizontal pressure gradient force directed onshore. In combination with the synoptic-scale horizontal pressure gradient force, this produced an ageostrophic southeasterly surface wind at LBA. Observations over land indicate the warming eventually continued above the cold layer, but was delayed after collapse of the mixed layer resulting from LBA at the surface. It is likely this upper

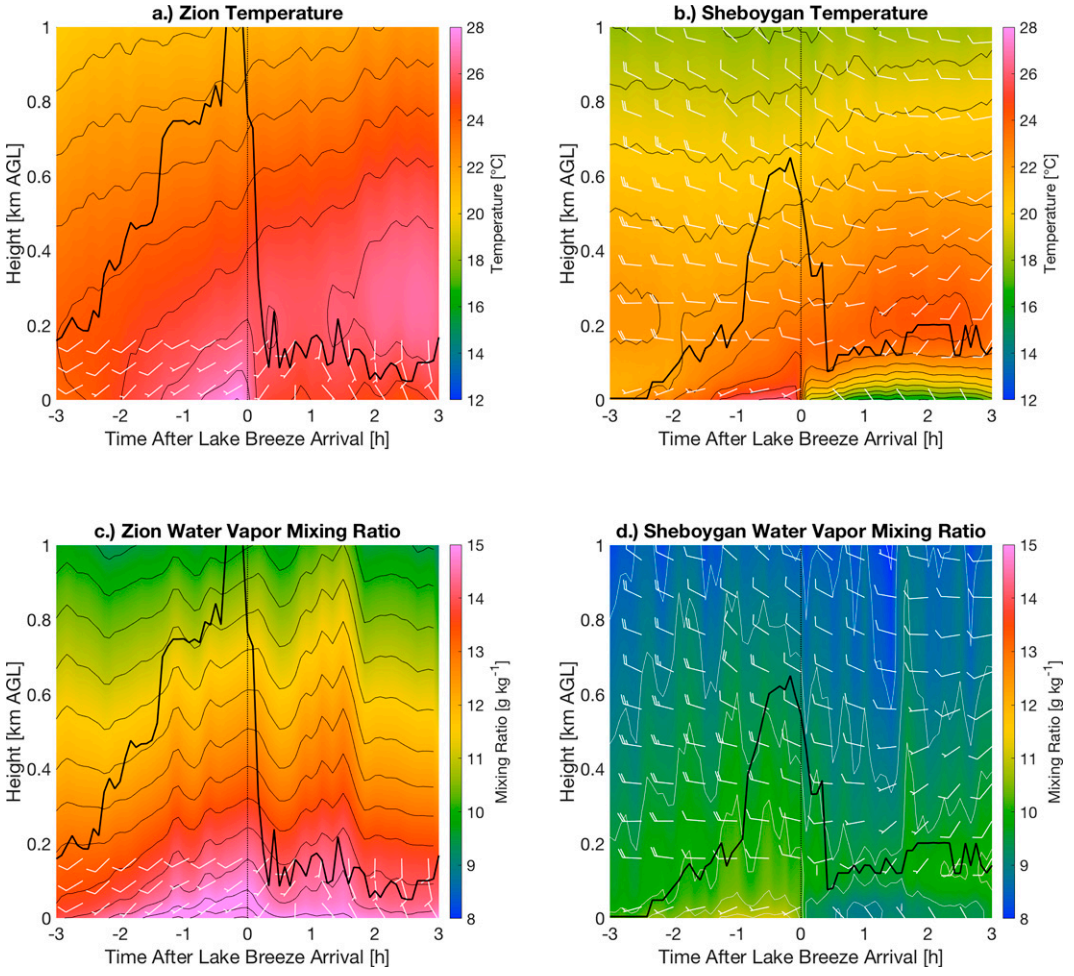

FIG. 3. Time–height cross sections of (top) temperature (°C) and (bottom) mixing ratio (g kg^{-1}) for (left) the microwave radiometer at Zion and (right) the AERI at Sheboygan. Winds observed by the sodar at Zion and the Doppler lidar at Sheboygan are overlaid on the respective plots. Winds are shown in knots (1 kt ≈ 0.51 m s^{-1}) using the standard convention; this unit was chosen over meters per second so that wind speed magnitudes would be large enough to be displayed with wind barbs. The 10-m surface winds at Sheboygan are appended at the bottom of the plot, but are displaced to the 30-m height for easier viewing. Temperature (mixing ratio) contours are every 1°C (0.5 g kg^{-1}). The thick black line represents the mixing depth calculated from the thermodynamic profiles.

warming over land was greater than above the lake. As a result, the onshore perturbation horizontal pressure gradient force also developed at upper levels, but later than at the surface. Therefore, one would expect a delay in the arrival of southeasterly winds at higher levels and a gradual upward slope to the advancing lake-breeze front.

Vertical profiles of the water vapor mixing ratio are also displayed in Fig. 3. It can be challenging to interpret remotely sensed profiles of moisture as the information content present in the infrared and microwave spectra for moisture is less than for temperature. Consequently, the vertical distribution of water vapor is not as clearly resolved as temperature. Due to these limitations it is likely that vertical gradients in moisture were actually greater than what is shown. Still, valuable insight can be obtained by inspecting the observations. Mixing ratio profiles at Sheboygan were markedly lower than at Zion, consistent with the surface observations. However, due to the lower temperature at Sheboygan, the relative humidity values (not shown) were of similar magnitude at the two sites. In the hours before LBA, warming-induced evaporation likely explains the observed increase in mixing ratio; simultaneously, the relative humidity was constant/decreasing with time as the effect of increased water vapor on relative humidity was outpaced by the higher temperatures. Following LBA, the mixing ratio observations in the lowest level of the profiles at the two sites were consistent with the values reported by the surface observations: nearly constant at Zion and slightly decreasing at Sheboygan.

The sodar and Doppler lidar clearly resolved the lower branch of the lake-breeze circulation. What is not clearly evident in these figures, however, is the presence of the upper-level return flow. While the 200-m vertical range of the Zion

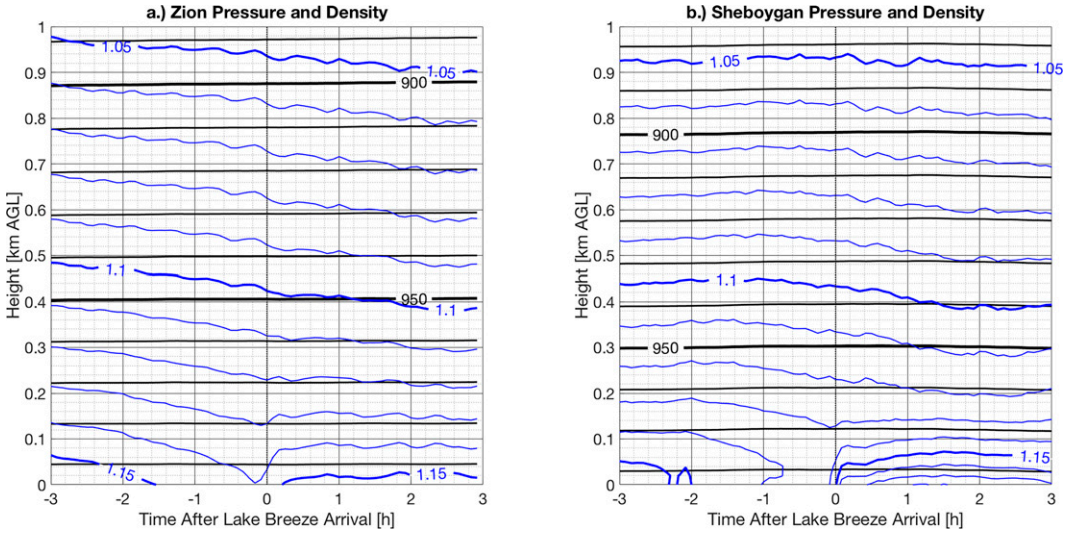

FIG. 4. Time–height cross sections of the mean pressure (black contours, hPa) and density (blue contours, kg m^{-3}) for (a) Zion and (b) Sheboygan. Pressure contours are drawn every 50 hPa and density contours are drawn every 0.05 kg m^{-3}.

sodar is likely too shallow, conceivably the lidar at Sheboygan could observe it since aircraft observations of a sea breeze by Finkele et al. (1995) showed return flow occurring between 700 and 1000 m. With easterly surface winds at Sheboygan post-LBA, one would expect corresponding westerly winds aloft that would augment the existing westerly flow, in which case the winds aloft would increase following LBA. However, Fig. 3 clearly shows that for the composite lake breeze presented here the westerly flow actually decreased in magnitude following LBA. An examination of the individual u wind components for each of the cases showed that the 12 June case may have exhibited return flow above 1.25 km; the other cases do not have lidar observations at that height due to a lack of sufficient aerosol scattering on those days. Lyons (1972) showed return flow for Chicago-area lake breezes tended to peak around 1500 m AGL. Therefore, the return flow in these cases may simply have been beyond the range of the lidar.

b. Baroclinicity and circulation

Time–height cross sections of pressure and density can be seen in Fig. 4. Since there are not corresponding high-temporal-resolution profiles over the lake, a definitive characterization of the baroclinicity of the environment cannot be made. However, the rate at which density changes relative to pressure can inform as to how quickly the environment is becoming more or less baroclinic. At the start of the analysis period, the isopycnals were parallel to isobars at all observed levels at Sheboygan, but daytime heating caused the density to change more quickly than the pressure. At Zion, the isobars and isopycnals were already intersecting at the start of the analysis, but the later LBA time means more heating has taken place. Below 300 m at Sheboygan (and throughout the entire depth of observations at Zion), the isopycnals slope downward in the time–height cross section, meaning that the atmosphere was becoming less dense with time as it approached LBA. At the same time, close inspection of Fig. 4 shows a slight upward slope in the isobars compared to the horizontal lines of the altitude grid. Once the lake breeze arrived, the slope of the isopycnals with respect to time reverses sign as the atmosphere rapidly became denser with arrival of the cold, dry air. After approximately one hour, the isopycnals and isobars were parallel again, consistent with a barotropic atmosphere. The density of the lake-breeze-advected air was greater at Sheboygan than at Zion, consistent with the disparity in temperatures between the two locations. When combined, the profiling observations at Sheboygan and Zion are consistent with the solenoidal characterization of lake-breeze circulations described earlier. It is important to note that the TROPoe retrieval algorithm derives the thermodynamic variables on a height grid and then calculates the pressure hypsometrically, which assumes that the atmosphere is in hydrostatic balance. While the small horizontal scale of sea breezes means that they do not necessarily behave hydrostatically, numerical modeling studies (e.g., Yang 1991) indicate that there is little difference between hydrostatic and nonhydrostatic simulations of weak sea breezes. Therefore, any error in the isobars in Fig. 4 due to a lack of hydrostatic balance is likely to be small.

The role of pressure and density in generating a lake breeze can be further explored by using Eq. (1) to calculate how the thermodynamic state at a given time forces changes in the circulation with time. Results using the composite AERI profiles at Sheboygan integrated over several different depths of the atmosphere are shown in Fig. 5. Regardless of the integration depth, the rate of change of circulation before LBA was close to zero or slightly

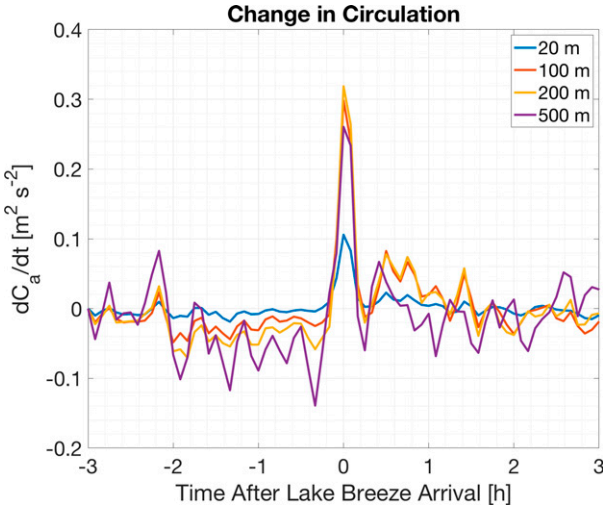

FIG. 5. Time series of the temporal rate of change in circulation as derived from AERI thermodynamic profiles. The circulation is evaluated over a layer that extends from the surface to the listed height.

negative. However, there was a substantial increase in the circulation rate at 0 h LBA, coincident with the observed shift in surface winds. This increase was visible at all analyzed heights, though the value for the 20-m layer was less than half of the values for the deeper layers. The values for 100- and 200-m depth were neutral to positive for 1.5 h after LBA, which indicates that the lake-breeze circulation continued to intensify after the time of LBA, coincident with the continued turning of the winds as observed by the DLID during that period. Altogether, these data are consistent with the theory that the lake breeze is actually a change in circulation that arises from local density differences. The observations at Zion (not shown) did not indicate similar behavior, although this is more likely an artifact of the coarse vertical resolution of the MWR rather than a product of any atmospheric difference at Zion.

c. Inland penetration and low-level structure

One of the ways in which individual lake-breeze events differ is the degree to which they penetrate inland. Certain lake breezes remain nearshore, impacting the conditions only within a few hundred meters of the shore or less, while others can extend hundreds of kilometers inland (Sills et al. 2011). To investigate the role of vertical structure on inland penetration, the events were classified into "near shore" or "inland" based on observed winds at inland sites. These inland observations came from two air quality monitoring sites operated by the Wisconsin Department of Natural Resources: Kenosha Water Tower, 5.7 km inland from the shore and 15 km northwest of Zion; and Sheboygan Haven, 5.3 km inland from the shore and 10 km northwest of Sheboygan. The locations of these sites relative to the Zion and Sheboygan supersites are marked in Fig. 1. If an observed wind at the inland site experienced a shift in wind direction that was consistent with the lake breeze for 3 h or more, it was considered to represent an inland lake-breeze event. Based on these criteria, three of the six events at Zion were classified as inland events while all but one event at Sheboygan were classified as such; these events are identified in Table 2 in bold type. To assess what, if any, role instability may have had in the penetration distance of the lake breezes, data from the AERI and MWR profilers were used to calculate the vertical rate of change of equivalent potential temperature θ_e. Results are displayed in Fig. 6. Positive (negative) values for $d\theta_e/dz$, representing convectively stable (unstable) conditions, are shaded in red (blue). While the small sample size makes it difficult to draw definitive conclusions, at least for the events observed here, the inland lake-breeze cases tended to form in more unstable environments (as evidenced by the blue shading above the near-surface layer) than the nearshore cases (which have more pink shading in the lowest 500 m). This is an interesting finding that stands in contrast to theory (Rotunno 1983; Walsh 1974), which states that the length scale of inland penetration of sea breezes is proportional to stability. However, modeling studies (e.g., Xian and Pielke 1991) have found that more unstable environments produce lake breezes with deeper penetrations. The Doppler lidar observations at Sheboygan indicated some correspondence between the strength of the preexisting westerly flow and whether a lake breeze penetrated inland or not, as the pre-LBA winds aloft in the sole nearshore case (12 June 2017) were stronger than the mean winds aloft of the inland cases. This is consistent with findings by Curry et al. (2017) and Mariani et al. (2018), who note that stronger offshore winds hinder the inland progression of the lake-breeze front. It may be that the preexisting flow, not the local convective stability, is the most important parameter for determining the degree of penetration. Doppler lidar observations at Sheboygan for the single nearshore case were absent for most of the post-LBA period. As a result, this study is unable to fully address the relative importance of stability versus wind speed in determining the degree of inland penetration.

The Zion sodar has a fine vertical resolution (10 m) and narrow dead band at the surface (30 m), and so it is well suited for investigating the structure of the lake breeze in greater detail. Figure 7 shows the time–height cross section of the mean zonal (u) and vertical (w) components of the sodar-observed winds during both the inland and nearshore cases; recall that there was an identical number (3) of events of each type at Zion. Since the shoreline at Zion is oriented in a due north–south direction, the u component of the wind effectively represents the cross-shore flow and a switch in the sign from positive to negative represents passage of the lake-breeze front. It is clear from the results that, regardless of breeze type, the lake-breeze front was a near-vertical wall approximately 100 m deep that arrived right at LBA and disrupted the predominately westerly flow. In the hours that follow, the nearshore cases exhibited little deepening from that initial impulse as the negative values for u were limited to the lowest 100 m of the troposphere. The inland cases, however, quickly grew to at least double their initial height. As noted

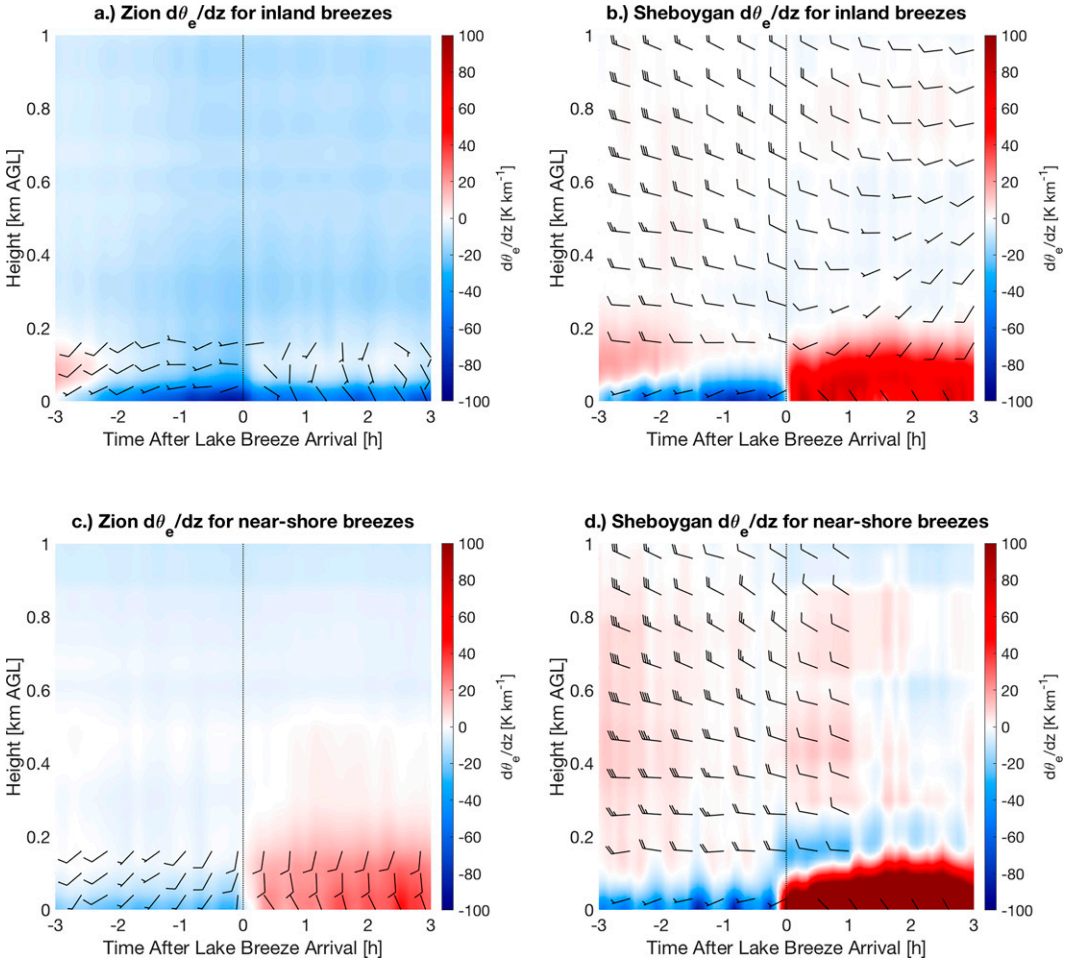

FIG. 6. Time–height cross sections of the vertical rate of change of the equivalent potential temperature θ_e for (top) inland breezes and (bottom) nearshore breezes at (left) Zion and (right) Sheboygan. Winds follow the same plotting convention as in Fig. 3.

above, the inland cases formed in more unstable environments. However, the contemporaneous vertical velocity observations indicated that thermodynamic instability was not likely to be the reason for the discrepancy in the two breeze types as the magnitudes of the vertical motion were largely similar during and following LBA for both breeze types. The strongest vertical lifting was found right at LBA as the arriving cold air acted as a density current and displaced the shoreline air upward. Following LBA, there is a hint of periodicity in the upward motion, especially in the nearshore (stable) cases (Fig. 7d) where positive vertical velocities are seen starting 30 min after LBA with a frequency of approximately 1 h. It is unlikely that these structures were thermals embedded in the convective boundary layer (as documented by Curry et al. 2017) as these occurred on a longer time scale and were the result of multiple cases being averaged together. Rather, they may represent a standing wave formed when the westerly preexisting flow collides with the dense air of the lake breeze. In this case, one would expect vertical velocity couplets in both nearshore and inland cases, but the pattern would be more pronounced in the nearshore cases due to their association with stronger westerly flow. The inland (unstable) cases tended toward more pronounced periods of vertical lift following LBA. However, these times were not well correlated with the vertical growth of the onshore flow. In fact, the lake breeze experienced its greatest vertical extent at the same time that the atmosphere was undergoing its most consistent period of subsidence. This tends to rule out momentum advection due to thermodynamic instability as a cause for growth of the lake-breeze layer. Since the MWR observations indicated the cold pool was not deepening with time, a more likely solution is that an onshore perturbation horizontal pressure gradient force had developed aloft, producing a sloped interface along the advancing lake-breeze front.

5. Aerosol impacts

The HSRL deployed at Sheboygan allowed for the observation of absolutely calibrated profiles of aerosol backscatter. Molecular backscattering often obscures the contributions of

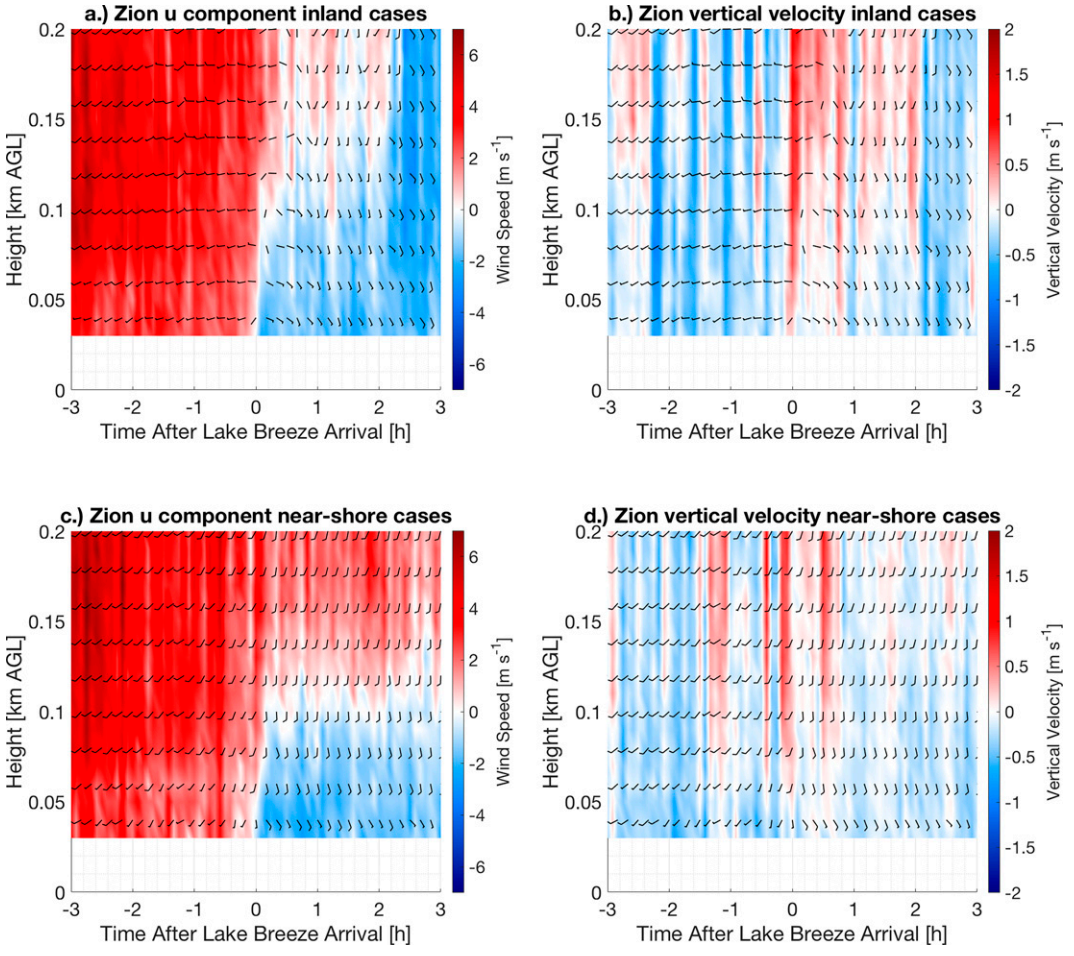

FIG. 7. Time–height cross sections of the sodar-observed (left) zonal (u) wind component and (right) vertical velocity at Zion for (top) inland and (bottom) nearshore lake breezes. Wind barbs are the two dimensional horizontal wind vectors(kt).

aerosols in traditional backscatter lidars, but the HSRL technique is able to separate and remove molecular scattering from the observed backscatter. During two of the six lake breezes observed at Sheboygan, enhanced aerosol backscatter was observed by the HSRL at the same altitude and time as the Doppler lidar observed the wind shift. These two cases can be seen in Fig. 8, which shows the time–height cross section of the base-10 logarithm of the aerosol backscatter cross section. In both cases (and in other cases not presented here) the growth of the boundary layer with solar heating can be seen as the increasing depth over which enhanced backscatter is visible starting before LBA but continuing after; this is especially apparent in the 2 June case in which the growth is easily visible starting nearly 3 h before LBA. After the growth in the depth of the lake breeze was significant enough that it could be observed by the Doppler lidar, both cases showed additional enhanced backscatter coincident with the shifting wind barbs, though it was more subtle on 2 June than 16 June. This is consistent with the lake breeze containing, on average, a slight enhancement in fine aerosols.

Increases in fine and ultrafine aerosol number concentrations were also observed around the time of LBA at Zion. Figure 9a shows the aerosol size distribution while Fig. 9b shows the times series of particulate matter with aerodynamic diameter less than 2.5 μm ($PM_{2.5}$). In the composite average, aerosols at sizes of 20–80 nm increased dramatically at the time of LBA. Similar graphs made for non-lake-breeze days (not shown) did not show the 20–80-nm enhancement. The mean quantitative increase in the total aerosol number was from 8413 cm^{-3} (pre-LBA) to 12 435 cm^{-3} (post-LBA), and was statistically significant using a two-sample t test. At the size where the post-LBA feature was most notable (38 nm), the size distribution function increased in height by a factor of 2.7.

Changes in other aerosol variables at Zion were investigated as well, including aerosol optical depth, integrated aerosol volume, and $PM_{2.5}$. As shown in Fig. 9b, for the 3-h period before LBA to the 3-h period after LBA, $PM_{2.5}$ increased by 2.5 $\mu g\ m^{-3}$ on lake-breeze days. This increase was greater than the increase on non-lake-breeze days (0.6 $\mu g\ m^{-3}$); for

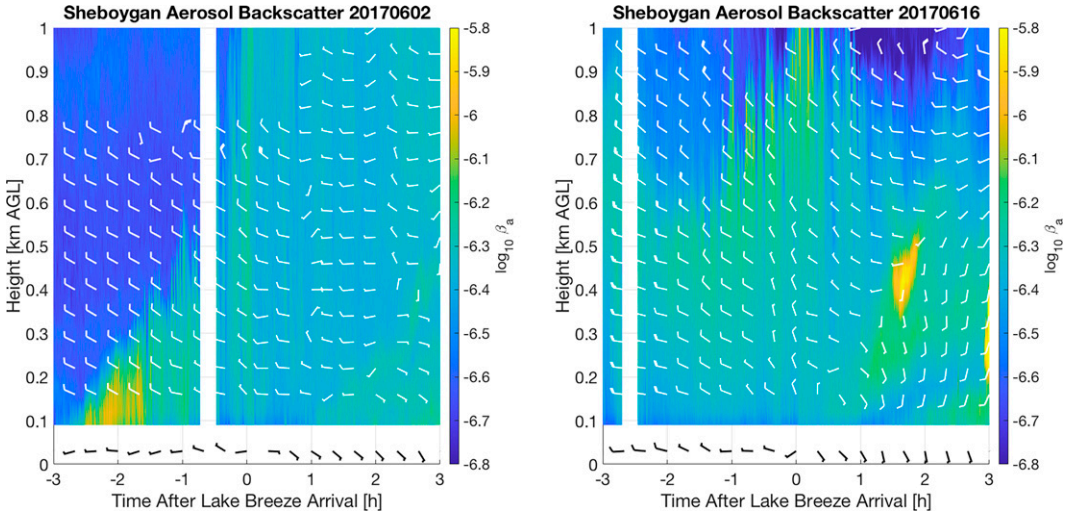

FIG. 8. Time–height cross section of aerosol backscatter for two lake-breeze cases from the High Spectral Resolution Lidar (HSRL) deployed at Sheboygan. White wind barbs are from the collocated Doppler lidar; black wind barbs are from the 10-m surface wind sensor but are plotted at 30 m to enhance readability. Wind barbs are in knots.

non-lake-breeze days, the average LBA time at Zion was used as the time to determine the relative difference. This difference was found to be statistically significant using a two-sample t test (p = 0.02). In situ integrated aerosol volume increased as well, consistent with the increases in aerosol number and $PM_{2.5}$. The increases in aerosol volume and $PM_{2.5}$ were not as distinct at the time of LBA as the change in ultrafine aerosol number, but rather suggested increasing mass of secondary aerosol in the air coming off the lake at later times in the day.

AOD at 550 nm on lake-breeze days (not shown) ranged from approximately 0.03 to 0.22, and AOD at 331 nm ranged from approximately 0.08 to 0.43. However, the AOD data were too sparse to create a composite time series or inspect for discontinuities at the LBA time. In a study in Toronto, increases in AOD and surface and vertical column density NO_2 were observed at LBA time (Davis et al. 2020), but direct comparisons cannot be drawn due to differences in land use, nearby sources, and fetch of the observation sites.

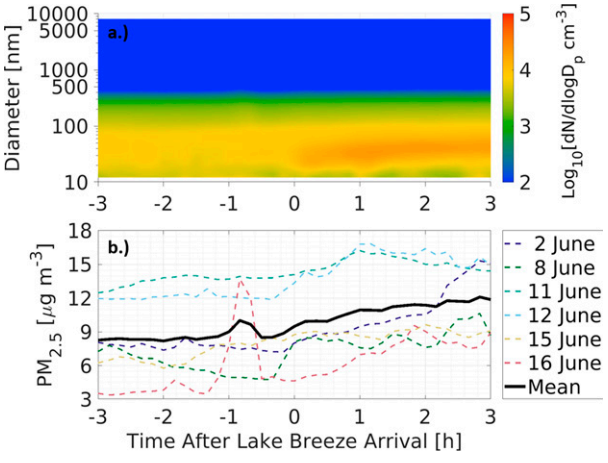

FIG. 9. (a) Average aerosol size distribution of all lake-breeze days (base-10 logarithm of cm^{-3}). (b) Time series of calculated $PM_{2.5}$ concentration ($\mu g\ m^{-3}$) relative to lake-breeze arrival time.

The general conceptual model of lake-breeze pollution episodes in the region (Dye et al. 1995), supported by LMOS 2017 results in Hughes et al. (2021) and Doak et al. (2021), suggest that much of the aerosol signal seen after LBA is due to anthropogenic pollution from land-based sources within the Lake Michigan airshed. Oxidation of precursor species leads to secondary aerosol formation in these plumes that are transported over the lake and then returned in the lake breeze. The conceptual model explains the gradual increase in aerosol volume and $PM_{2.5}$ seen after LBA, and the greater increase (afternoon versus morning) on lake-breeze days versus non-lake-breeze days. However, the conceptual model does not explain the distinct increase in ultrafine aerosol seen at the LBA time. This is consistent with ultrafine aerosols generating from breaking of freshwater waves (Slade et al. 2010; Axson et al. 2016); however, combustion sources over the lake, gas-to-particle nucleation over the lake (likely in land-based anthropogenic plumes), and other potential sources are possible. Other observations such as time-resolved measurements of wave state, ultrafine aerosol chemistry, and vertical profiles of aerosols would be required to elucidate specific contributions.

6. Synthesis and conclusions

As part of the 2017 Lake Michigan Ozone Study, ground-based supersites were deployed at two locations adjacent to the western shore of Lake Michigan. The unique combination of kinematic and thermodynamic profilers at each site enabled the analysis of lake-breeze structure in unprecedented detail, and a compelling portrait of the development

of this phenomenon emerged from the synthesis of these instruments and surface measurements.

These observations show that lake breezes during LMOS 2017 developed as follows. In the absence of synoptic forcing, a preexisting inversion was present over the land in the overnight hours with predominately westerly flow throughout the lower troposphere. Background aerosol concentrations showed little difference from average values during this time of the year. Following sunrise, several significant changes began to take place in the lower troposphere. Over the next three to four hours solar heating increased the surface temperature and the depth of the PBL while increased mixing eroded the previous inversion; analysis of the potential temperature profiles (not shown) revealed that the lower PBL becomes largely isentropic with height during this time. While the air over land warmed, the temperature of the air over the lake remained largely unchanged. As a result, the density of the air over land became much less than over water, resulting in sloping isopycnals as observed by the thermodynamic profilers and an increase in baroclinicity. Since the change in the circulation around a fluid element is a function of the magnitude of the baroclinicity, a circulation in the vertical plane developed that was superimposed over the preexisting westerly flow. Up to this point, there was little change in the wind as the preexisting circulation in the vertical plane was small. However, the baroclinic forcing resulted in a sudden increase in the circulation which manifested itself as the lake breeze. The change in circulation derived from baroclinicity was well captured by the ground-based profilers.

The lake-breeze front was on the order of 100–200 m deep and represents the leading edge of the air that has been cooled by conduction of heat into Lake Michigan. This air mass was advected over the land by the lower branch of the lake-breeze circulation, and as it advanced it forced an updraft on the order of 1–2 m s^{-1}. The concentration of aerosols having a diameter of 20–80 nm increased to nearly an order of magnitude above background levels with passage of the lake-breeze front. While the change in $PM_{2.5}$ concentration was not as dramatic, it still showed a marked increase after the lake-breeze front. The low-level relative humidity over land increased with the passage of the lake-breeze front, even as the absolute humidity was steady or even decreasing, owing to the significant decrease in temperature. Changes in the local thermodynamics resulted in decreased baroclinicity in the lower troposphere, and the lake-breeze circulation achieved a steady state within a few minutes with little change in wind speed or direction observed in the lowest 100 m after that time.

The local near-surface environment had been generally stabilized by the lake breeze as evidenced by strong increases in potential temperature with height in the lowest 100–200 m. The advancing cold air undercut the warm air over land and lifted it, creating a strong inversion on the order of 8 K over just 200 m. While the aforementioned lifting can force cloud development along the lake-breeze front, the strong stabilization of the atmosphere behind the front resulted in clearing skies, as seen in the satellite imagery in Fig. 1.

Some questions remain about the reasons behind the different characteristics observed at the two sites. For example, the difference between the air and lake temperatures was nearly identical between the two sites in the period leading up to LBA, but there was substantial divergence in the temperature differences following LBA as the ensuing gradient was twice as strong at Zion as at Sheboygan. At the same time, the absolute moisture content of the air at Zion seemed to be unaffected by the lake breeze while it dropped by nearly half at Sheboygan. It is important to remember that there are slight differences in the set of cases used for analysis, as both the coldest-day pre-LBA at Sheboygan and the warmest-day post-LBA at Zion were the two event days on which there was no corresponding breeze at the other site. This would help bias the respective sites in opposite directions. The two sites themselves were not situated identically, either, as the Sheboygan site was much closer to the shore than the Zion site (230 m vs 1 km). The longer fetch at Zion combined with the relatively slow speed at which lake-cooled air is advected over the warmer land means that the air can undergo substantially more modification at that site than Sheboygan. The degree of urban development also provides an interesting contrast between the two sites. At the microscale, the Sheboygan site was more urbanized as it was deployed next to a resort development while the Zion site was within a state park. However, the community of Sheboygan is a discrete smaller city surrounded by farmland while Zion is in the heart of the urban amalgamation that lies between Chicago and Milwaukee. The degree to which these different settings may impact the characteristics of the lake breeze is an important question, but one that is beyond the scope of the present work.

This work covers a relatively small number of cases along one shore of just one of the Great Lakes. Additional observations at other locations are needed to determine if the behaviors observed here are also seen at bodies of water with different shoreline geometries, surface area, water depths, climate regimes, and other qualities that can impact water–land–atmosphere interactions. For future observational studies of lake- or sea-breeze structure, an ideal observing site would contain both a sodar and a Doppler lidar so that a more complete profile of winds over the lowest kilometer of the atmosphere could be observed since the sodar would fill in all but the very lowest level of the lidar's dead band. When coupled with an AERI and in situ surface meteorology sensors, this would provide a near-continuous profile of atmospheric thermodynamics and kinematics from the surface to the maximum effective range of the lidar.

Acknowledgments. The authors are indebted to David Turner, who assisted with applying the TROPoe algorithm to the microwave radiometer data. Steve Smith assisted with deployment of the radiometer and sodar at Zion while Erik Olson led the deployment of SPARC at Sheboygan. David Loveless and Coda Phillips (University of Wisconsin–Madison) and Jack Bruno (Ohio University) monitored the SPARC. Funding for the SPARC trailer

deployment and the University of Northern Iowa's participation at Zion during LMOS 2017 was provided by the GOES-R Program Office via the NOAA Cooperative Agreement with the Cooperative Institute for Meteorological Satellite Studies (NA15NES432001). The three anonymous reviewers contributed many insightful comments and suggestions that greatly improved this paper. This work was funded in part by the National Science Foundation under Grants AGS-1712909, AGS-1713001, and AGS-1712828.

Data availability statement. Profiler data used in this study are freely available from the LMOS 2017 campaign archive at https://www-air.larc.nasa.gov/missions/lmos/index.html. Inland wind observations were obtained from the EPA Air Quality System at https://aqs.epa.gov/aqs/.

REFERENCES

Abdioskouei, M., and Coauthors, 2019: 2017 Lake Michigan Ozone Study (LMOS) preliminary finding report. LMOS Rep., 105 pp., https://www.ladco.org/wp-content/uploads/Research/LMOS2017/LMOS_LADCO_report_revision_apr2019_final.pdf.

Axson, J. L., N. W. May, I. D. Colon-Bernal, K. A. Pratt, and A. P. Ault, 2016: Lake spray aerosol: A chemical signature from individual ambient particles. *Environ. Sci. Technol.*, **50**, 9835–9845, https://doi.org/10.1021/acs.est.6b01661.

Banta, R. M., L. D. Olivier, and D. H. Levinson, 1993: Evolution of the Monterey Bay sea-breeze layer as observed by a pulsed Doppler lidar. *J. Atmos. Sci.*, **50**, 3959–3982, https://doi.org/10.1175/1520-0469(1993)050<3959:EOTMBS>2.0.CO;2.

Blumberg, W. G., D. D. Turner, U. Löhnert, and S. Castleberry, 2015: Ground-based temperature and humidity profiling using spectral infrared and microwave observations. Part II: Actual retrieval performance in clear-sky and cloud conditions. *J. Appl. Meteor. Climatol.*, **54**, 2305–2319, https://doi.org/10.1175/JAMC-D-15-0005.1.

Curry, M., J. Hanesiak, S. Kehler, D. M. L. Sills, and N. M. Taylor, 2017: Ground-based observations of the thermodynamic and kinematic properties of lake-breeze fronts in southern Manitoba, Canada. *Bound.-Layer Meteor.*, **163**, 143–159, https://doi.org/10.1007/s10546-016-0214-1.

Davis, Z. Y. W., D. M. L. Sills, and R. McLaren, 2020: Enhanced NO_2 and aerosol extinction observed in the tropospheric column behind lake-breeze fronts using MAX-DOAS. *Atmos. Environ.*, **5**, 100066, https://doi.org/10.1016/j.aeaoa.2020.100066.

Doak, A. G., and Coauthors, 2021: Characterization of ground-based atmospheric pollution and meteorology sampling stations during the Lake Michigan Ozone Study 2017. *J. Air Waste Manage. Assoc.*, **71**, 866–889, https://doi.org/10.1080/10962247.2021.1900000.

Dye, T. S., P. T. Roberts, and M. E. Korc, 1995: Observations of transport processes for ozone and ozone precursors during the 1991 Lake Michigan Ozone Study. *J. Appl. Meteor.*, **34**, 1877–1889, https://doi.org/10.1175/1520-0450(1995)034<1877:OOTPFO>2.0.CO;2.

Ebell, K., E. Orlandi, A. Hünerbein, U. Löhnert, and S. Crewell, 2013: Combining ground-based with satellite-based measurements in the atmospheric state retrieval: Assessment of the information content. *J. Geophys. Res. Atmos.*, **118**, 6940–6956, https://doi.org/10.1002/jgrd.50548.

Eloranta, E. W., 2005: High Spectral Resolution Lidar. *Lidar: Range-Resolved Optical Remote Sensing of the Atmosphere*, K. Weitkamp, Ed., Springer, 143–163.

Finkele, K., J. M. Hacker, H. Kraus, and R. A. D. Byron-Scott, 1995: A complete sea-breeze circulation cell derived from aircraft observations. *Bound.-Layer Meteor.*, **73**, 299–317, https://doi.org/10.1007/BF00711261.

Herman, J., A. Cede, E. Spinei, G. Mount, M. Tzortziou, and N. Abuhassan, 2009: NO_2 column amounts from ground-based Pandora and MFDOAS spectrometers using the direct-sun DOAS technique: Intercomparisons and application to OMI validation. *J. Geophys. Res.*, **114**, D13307, https://doi.org/10.1029/2009JD011848.

Holben, B. N., and Coauthors, 1998: AERONET—A federated instrument network and data archive for aerosol characterization. *Remote Sens. Environ.*, **66**, 1–16, https://doi.org/10.1016/S0034-4257(98)00031-5.

Holton, J., 1992: *An Introduction to Dynamic Meteorology*. 3rd ed. Academic Press, 511 pp.

Hughes, D. D., and Coauthors, 2021: $PM_{2.5}$ chemistry, organosulfates, and secondary organic aerosol during the 2017 Lake Michigan Ozone Study. *Atmos. Environ.*, **244**, 117939, https://doi.org/10.1016/j.atmosenv.2020.117939.

Keen, C. S., and W. A. Lyons, 1978: Lake/land breeze circulations on the western shore of Lake Michigan. *J. Appl. Meteor.*, **17**, 1843–1855, https://doi.org/10.1175/1520-0450(1978)017<1843:LBCOTW>2.0.CO;2.

Khlystov, A., C. Stanier, and S. N. Pandis, 2004: An algorithm for combining electrical mobility and aerodynamic size distributions data when measuring ambient aerosol. *Aerosol Sci. Technol.*, **38**, (Suppl.) 229–238, https://doi.org/10.1080/02786820390229543.

King, P. W. S., M. J. Leduc, D. M. L. Sills, N. R. Donaldson, D. R. Hudak, P. Joe, and P. B. Murphy, 2003: Lake breezes in southern Ontario and their relation to tornado climatology. *Wea. Forecasting*, **18**, 795–807, https://doi.org/10.1175/1520-0434(2003)018<0795:LBISOA>2.0.CO;2.

Knuteson, R. O., and Coauthors, 2004a: Atmospheric emitted radiance interferometer. Part I: Instrument design. *J. Atmos. Oceanic Technol.*, **21**, 1763–1776, https://doi.org/10.1175/JTECH-1662.1.

——, and Coauthors, 2004b: Atmospheric emitted radiance interferometer. Part II: Instrument performance. *J. Atmos. Oceanic Technol.*, **21**, 1777–1789, https://doi.org/10.1175/JTECH-1663.1.

Laird, N., D. R. Kristovich, X.-Z. Liang, R. W. Arritt, and K. Labas, 2001: Lake Michigan lake breezes: Climatology, local forcing, and synoptic environment. *J. Appl. Meteor.*, **40**, 409–424, https://doi.org/10.1175/1520-0450(2001)040<0409:LMLBCL>2.0.CO;2.

Levy, I., and Coauthors, 2010: Unravelling the complex local-scale flows influencing ozone patterns in the southern Great Lakes of North America. *Atmos. Chem. Phys.*, **10**, 10 895–10 915, https://doi.org/10.5194/acp-10-10895-2010.

Loveless, D. M., T. J. Wagner, D. D. Turner, S. A. Ackerman, and W. F. Feltz, 2019: A composite perspective on bore passages during the PECAN campaign. *Mon. Wea. Rev.*, **147**, 1395–1413, https://doi.org/10.1175/MWR-D-18-0291.1.

Lyons, W. A., 1970: Numerical simulation of Great Lakes summertime conduction inversions. *Proc. 13th Conf. on Great*

Lakes Research, Buffalo, NY, International Association for Great Lakes Research, 369–387.

——, 1972: The climatology and prediction of the Chicago lake breeze. *J. Appl. Meteor.*, **11**, 1259–1270, https://doi.org/10.1175/1520-0450(1972)011<1259:TCAPOT>2.0.CO;2.

——, and H. S. Cole, 1976: Photochemical oxidant transport: Mesoscale lake breeze and synoptic-scale aspects. *J. Appl. Meteor.*, **15**, 733–743, https://doi.org/10.1175/1520-0450(1976)015<0733:POTMLB>2.0.CO;2.

Mariani, Z., A. Dehghan, P. Joe, and D. Sills, 2018: Observations of lake-breeze events during the Toronto 2015 Pan-American Games. *Bound.-Layer Meteor.*, **166**, 113–135, https://doi.org/10.1007/s10546-017-0289-3.

Martin, J. E., 2006: *Mid-Latitude Atmospheric Dynamics: A First Course.* Wiley, 324 pp.

Mastrantonio, G., and Coauthors, 1994: Observations of sea breeze events in Rome and the surrounding area by a network of Doppler sodars. *Bound.-Layer Meteor.*, **71**, 67–80, https://doi.org/10.1007/BF00709220.

Miller, S. T. K., B. D. Keim, R. W. Talbot, and H. Mao, 2003: Sea breeze: Structure, forecasting, and impacts. *Rev. Geophys.*, **41**, 1011, https://doi.org/10.1029/2003RG000124.

Pearson, G., F. Davies, and C. Collier, 2009: An analysis of the performance of the UFAM pulsed Doppler lidar for observing the boundary layer. *J. Atmos. Oceanic Technol.*, **26**, 240–250, https://doi.org/10.1175/2008JTECHA1128.1.

Prakash, J. W. J., R. Ramachandran, K. N. Nair, K. S. Gupta, and P. K. Kunhikrishnan, 1992: On the structure of sea-breeze fronts observed near the coastline of Thumba, India. *Bound.-Layer Meteor.*, **59**, 111–124, https://doi.org/10.1007/BF00120689.

Rotunno, R., 1983: On the linear theory of the land and sea breeze. *J. Atmos. Sci.*, **40**, 1999–2009, https://doi.org/10.1175/1520-0469(1983)040%3C1999:OTLTOT%3E2.0.CO;2.

Ryznar, E., and J. S. Touma, 1981: Characteristics of true lake breezes along the eastern shore of Lake Michigan. *Atmos. Environ.*, **15**, 1201–1205, https://doi.org/10.1016/0004-6981(81)90311-5.

Schwab, D. J., G. A. Keshkevich, and G. C. Muhr, 1999: Automated mapping of surface water temperature in the Great Lakes. *J. Great Lakes Res.*, **25**, 468–481, https://doi.org/10.1016/S0380-1330(99)70755-0.

Scott, R. W., and F. A. Huff, 1996: Impacts of the Great Lakes on regional climate conditions. *J. Great Lakes Res.*, **22**, 845–863, https://doi.org/10.1016/S0380-1330(96)71006-7.

Segal, M., M. Leuthold, R. W. Arritt, C. Andersen, and J. Shen, 1997: Small lake daytime breezes: Some observational and conceptual evaluations. *Bull. Amer. Meteor. Soc.*, **78**, 1135–1147, https://doi.org/10.1175/1520-0477(1997)078<1135:SLDBSO>2.0.CO;2.

Shen, S., P. A. Jacques, Y. Zhu, M. D. Geller, and C. Sioutas, 2002: Evaluation of the SMPS-APS system as a continuous monitor for measuring $PM_{2.5}$, PM_{10}, and coarse ($PM_{2.5-10}$) concentrations. *Atmos. Environ.*, **36**, 3939–3950, https://doi.org/10.1016/S1352-2310(02)00330-8.

Shipley, S. T., D. H. Tracy, E. W. Eloranta, J. T. Trauger, J. T. Sroga, F. L. Roesler, and J. A. Weinman, 1983: High Spectral Resolution Lidar to measure optical scattering properties of atmospheric aerosols 1: Theory and instrumentation. *Appl. Opt.*, **22**, 3716–3724, https://doi.org/10.1364/AO.22.003716.

Sills, D. M., J. R. Brook, I. Levy, P. A. Makaer, J. Zhang, and P. A. Taylor, 2011: Lake breezes in the southern Great Lakes region and their influence during BAQS-Met 2007. *Atmos. Chem. Phys.*, **11**, 7955–7973, https://doi.org/10.5194/acp-11-7955-2011.

Simpson, J. E., 1994: *Sea Breeze and Local Wind.* Cambridge University Press, 244 pp.

Slade, J. H., T. M. VanReken, G. R. Mwaniki, S. Bertman, B. Stirm, and P. B. Shepson, 2010: Aerosol production from the surface of the Great Lakes. *Geophys. Res. Lett.*, **37**, L18807, https://doi.org/10.1029/2010GL043852.

Smirnov, A., B. N. Holben, T. F. Eck, O. Dubovik, and I. Slutsker, 2000: Cloud-screening and quality control algorithms for the AERONET database. *Remote Sens. Environ.*, **73**, 337–349, https://doi.org/10.1016/S0034-4257(00)00109-7.

Stanier, C. O., and Coauthors, 2021: Overview of the Lake Michigan Ozone Study 2017. *Bull. Amer. Meteor. Soc.*, **102**, E2207–E2225, https://doi.org/10.1175/BAMS-D-20-0061.1.

Turner, D. D., and U. Löhnert, 2014: Information content and uncertainties in thermodynamic profiles and liquid cloud properties retrieved from the ground-based Atmospheric Emitted Radiance Interferometer (AERI). *J. Appl. Meteor. Climatol.*, **53**, 752–771, https://doi.org/10.1175/JAMC-D-13-0126.1.

——, and W. G. Blumberg, 2019: Improvements to the AERIoe thermodynamic profile retrieval algorithm. *IEEE J. Sel. Top. Appl. Earth Obs. Remote Sens.*, **12**, 1339–1354, https://doi.org/10.1109/JSTARS.2018.2874968.

——, and U. Löhnert, 2021: Ground-based temperature and humidity profiling: Combining active and passive remote sensors. *Atmos. Meas. Tech.*, **14**, 3033–3048, https://doi.org/10.5194/amt-14-3033-2021.

——, R. O. Knuteson, H. E. Revercomb, C. Lo, and R. G. Dedecker, 2006: Noise reduction of Atmospheric Emitted Radiance Interferometer (AERI) observations using principal component analysis. *J. Atmos. Oceanic Technol.*, **23**, 1223–1238, https://doi.org/10.1175/JTECH1906.1.

Vermeuel, M. P., and Coauthors, 2019: Sensitivity of ozone production to NO*x* and VOC along the Lake Michigan coastline. *J. Geophys. Res. Atmos.*, **124**, 10 989–11 006, https://doi.org/10.1029/2019JD030842.

Wagner, T. J., W. F. Feltz, and S. A. Ackerman, 2008: The temporal evolution of convective indices in storm-producing environments. *Wea. Forecasting*, **23**, 786–794, https://doi.org/10.1175/2008WAF2007046.1.

——, D. D. Turner, and P. M. Klein, 2019: A new generation of ground-based mobile platforms for active and passive profiling of the atmospheric boundary layer. *Bull. Amer. Meteor. Soc.*, **100**, 137–153, https://doi.org/10.1175/BAMS-D-17-0165.1.

Walsh, J. E., 1974: Sea breeze theory and applications. *J. Atmos. Sci.*, **31**, 2012–2026, https://doi.org/10.1175/1520-0469(1974)031<2012:SBTAA>2.0.CO;2.

Xian, Z., and R. A. Pielke, 1991: The effects of width of land masses on the development of sea breezes. *J. Appl. Meteor.*, **30**, 1280–1304, https://doi.org/10.1175/1520-0450(1991)030<1280:TEOWOL>2.0.CO;2.

Yang, X., 1991: A study of nonhydrostatic effects in idealized sea breeze systems. *Bound.-Layer Meteor.*, **54**, 183–208, https://doi.org/10.1007/BF00119419.